# *Boosting the electrochemical performance of Li-garnet based all-solid-state batteries with Li[subscript 4]Ti[subscript 5]O[subscript 12] electrode: Routes to cheap and large scale ceramic processing*



**Citation:** Van den Broek, Jan, Jennifer L. M. Rupp, and Semih Afyon. "Boosting the Electrochemical Performance of Li-Garnet Based All-Solid-State Batteries with Li4Ti5O12 Electrode: Routes to Cheap and Large Scale Ceramic Processing." Journal of Electroceramics 38, no. 2–4 (April 11, 2017): 182–188.

**As Published:** http://dx.doi.org/10.1007/s10832-017-0079-9

**Publisher:** Springer US

**Persistent URL:** http://hdl.handle.net/1721.1/113603

**Version:** Author's final manuscript: final author's manuscript post peer review, without publisher's formatting or copy editing

DOI: 10.1002/ ((please add manuscript number))

**Article type:** Full Paper

# Boosting the Electrochemical Performance of Li-Garnet based All-Solid-State Batteries with $Li_4Ti_5O_{12}$ Electrode: Routes to Cheap and Large Scale Ceramic Processing

*By Semih Afyon*[a], Jan van den Broek[a], Jennifer L. M. Rupp*[a, b]*

((Optional Dedication))

[a] Electrochemical Materials, ETH Zurich, 8093 Zurich, Switzerland
[b] Electrochemical Materials Labs, Massachusetts Institute of Technologies (MIT), Cambridge, Massachusetts 02139, United States of America

Corresponding authors:
E-mail: semih.afyon@alumni.ethz.ch
jrupp@mit.edu

**Keywords:** Li-ion Batteries, Solid Electrolyte, Garnet, Ionic Conductivity, Al doped $Li_7La_3Zr_2O_{12}$, $Li_4Ti_5O_{12}$, anode

**Abstract**

All-solid-state batteries based on fast $Li^+$ conducting solid electrolytes such as $Li_7La_3Zr_2O_{12}$ (LLZO) give perspective on safe, non-inflammable, and temperature tolerant energy storage. Despite the promise, ceramic processing of whole battery assemblies reaching close to theoretical capacities and finding optimal strategies to process large-scale and low cost battery cells remains a challenge. Here, we tackle these issues and report on a solid-state battery cell composed of $Li_4Ti_5O_{12}$ / c-$Li_{6.25}Al_{0.25}La_3Zr_2O_{12}$ / metallic Li delivering capacities around 70-75 Ah/kg with reversible cycling at a rate of 8 A/kg (for 2.5-1.0 V, 95 $^oC$). A key aspect towards the increase in capacity and $Li^+$ transfer at the solid electrolyte-electrode interface is found to be the intimate embedding of grains and their connectivity, which can be implemented by the isostatic pressing of cells during their preparation. We suggest that simple adaption of ceramic processing, such as the applied pressure during processing, strongly alters the electrochemical performance by assuring good grain contacts at the electrolyte-electrode interface. Among the garnet-type all-solid-state ceramic battery assemblies in the field, considerably improved capacities and cycling properties are demonstrated for $Li_4Ti_5O_{12}$ / c-$Li_{6.25}Al_{0.25}La_3Zr_2O_{12}$ / metallic Li pressed cells, giving new perspectives on cheap ceramic processing and up-scalable garnet-based all-solid-state batteries.

## 1. Introduction

Li-ion batteries are the predominant battery technology at present due their high energy density, long cycle life, and variable charge/discharge rates [1-3]. However, liquid organic electrolytes used in Li-ion batteries pose safety issues due to their flammability and potential leakage risk. The generally low chemical stability of liquid electrolytes also greatly limits the selection of electrode materials that can be used. All-solid-state batteries would enable the use of novel types of electrode materials on both at the cathode and anode side that are conventionally not stable with liquid electrolytes. Considering the cathode side, for example sulfur [4], manganese [5-7], or vanadate [8, 9] based novel electrode materials could be utilized, which offer increased capacity but are known to show long term stability issues with conventional liquid electrolytes [10]. For the anode, a solid electrolyte could enable the use of elemental lithium by preventing, or at least strongly reducing, dendritic lithium growth and enable higher energy densities and voltages. Other important advantages include the higher chemical and thermal stability of solid electrolytes when compared to many organic liquids. This not only makes it possible to use and cycle Li-ion batteries at elevated temperatures, i.e., in combination with thermal waste heat recovery, but also increases safety in general. In addition, all-solid-state battery concepts allow for the miniaturization of battery systems to high energy density microbatteries (a.k.a. thin-film batteries). This would enable a manifold of new applications, for example for portable electronics, medical devices, or batteries directly integrated in electronic circuits [11-13] such as autonomous power units coupled with a memory or sensing unit on future Si chip architectures [14, 15].

Today, many different inorganic solid Li-ion electrolytes have been investigated showing a wide range of Li-ionic conductivities, chemical stability, and phase stability, see reviews by Cao et al. [16], Knauth et al. [17], and the recent in depth review by Janek and Zeier [18]. Among the plethora of solid state electrolytes, garnet-type $Li_7La_3Zr_2O_{12}$ (LLZO) has lately received considerable attention, being first synthesized and characterized by Murugan et al. in

2007 [19]. In the high conducting phase, LLZO exhibits a remarkable Li-ion conductivity of up to $10^{-3}$ S/cm at room temperature and a high chemical stability towards metallic lithium [19-22]. LLZO shows its high Li-ion conductivity only in its cubic phase polymorph, which must be stabilized at room temperature by the introduction of extrinsic dopants. The effect of different doping strategies and processing conditions on the resulting phase purity, sintering density, and Li-ion conductivity has been investigated for pellets and thin films, see Refs. [23-33] for details. However, there exist only a handful of investigations going one step further into the deposition of electrodes onto the LLZO electrolyte and the electrochemical testing and characterization of full battery cells. This includes the investigation of different deposition techniques of the electrodes, the effect of electrode composition, the resistivity of the solid electrolyte-electrode interface, and the chemical stability of electrolyte, electrode and electrolyte-electrode interface during cycling of full battery cells. Very recently, we summarized state-of-the-art battery capacities reported for all-solid-state Li batteries based on LLZO electrolyte for various tested electrode materials, see van den Broek et al. for details [32]. It can be noted that LLZO-based solid-state Li-ion batteries are combined with either the cathode material $LiCoO_2$ [22, 34-38] or $LiMn_{1.5}Ni_{0.5}O_4$ [39], or on the anode side with $Li_4Ti_5O_{12}$ [32]. Up to date, capacities close to theoretical ones have only been achieved for battery cells, in which the electrode material has been deposited as a thin-film onto the LLZO electrolyte, see reports by Ohta et al. [34, 35] and Kato et al. [38]. This can be explained by the very good contact between the solid-state electrolyte and electrode forming a low interfacial resistance, the very low electrode thickness (< 1 µm), and the high purity and quality of the electrode layer after deposition in vacuum such as done with PLD [34, 35, 38]. However, for the large-scale industrial realization of all-solid-state batteries with LLZO electrolyte, cheap and alternative processing methods have to be found utilizing direct casting of electrode materials, additives, and binders onto the LLZO electrolyte. Reviewing previous reports, it can be stated that all-solid-state batteries prepared by classic large-scale ceramic

processing have still challenges in assuring a low contact resistance and require additional co-sintering of the solid electrolyte and electrode [22, 36, 37]. Recently, we deposited $Li_4Ti_5O_{12}$ anodes onto sintered LLZO electrolyte pellet surfaces by direct casting of an electrode slurry, in the same way as electrodes are deposited for Li-ion batteries with liquid electrolyte, resulting in thick electrode layers of ~25 µm and a good mechanical contact at the electrolyte-electrode interface [32]. Additionally, the accessible capacity of the all-solid-state battery cells could be greatly increased by fabricating a porous electrolyte layer onto the dense LLZO pellets into which the $Li_4Ti_5O_{12}$ electrode slurry was immersed, resulting in a much better interface contact [32]. It could be inferred from this work that the choice in ceramic processing of the electrolyte–electrode interface is of great importance to reach the goal of cyclable and high capacity all-solid-state Li-ion batteries, as it largely defines the contact area and $Li^+$ transfer kinetics.

In this work, we take a different approach to this problem and report on the effect of isostatic pressing of the solid electrolyte–electrode interface on the electrochemical properties of full all-solid-state Li-ion batteries. Cells with a configuration of $Li_4Ti_5O_{12}$ / c-$Li_{6.25}Al_{0.25}La_3Zr_2O_{12}$ / metallic Li are fabricated by direct casting of an electrode slurry onto dense LLZO pellet surfaces followed by isostatic pressing. Such cells show reversible charge–discharge behavior and stable cycling at slightly elevated temperatures of 75–95 °C. In comparison to non-pressed cells, the pressed-cells show much improved electrochemical performance and deliver considerably higher discharge capacities. The new processing and assembly method presented here enables new pathways and options for future investigations and practical applications of all-solid-state batteries based on garnet-type cubic $Li_7La_3Zr_2O_{12}$ (LLZO) structures.

## 2. Experimental Section

*Synthesis, Powder, and Pellet Processing of the c-$Li_{6.25}Al_{0.25}La_3Zr_2O_{12}$ Solid Electrolyte:* For the synthesis of cubic particles with composition c-$Li_{6.25}Al_{0.25}La_3Zr_2O_{12}$, stoichiometric amounts of $LiNO_3$ (99 %, Alfa Aesar), $Al(NO_3)_3 \cdot 9H_2O$ (99 %, Fluka Chemika), $La(NO_3)_3 \cdot 6H_2O$ (99.9 %, Alfa Aesar), and zirconium(IV) acetylacetonate (98 %, abcr) were dissolved in a solvent mixture of ethanol and water at elevated temperatures. After evaporation of the solvent, the dried xerogel was calcined in aluminum crucibles at 650 °C for 15 h under a constant synthetic air flow. The resulting c-$Li_{6.25}Al_{0.25}La_3Zr_2O_{12}$ powder (see **Supplementary Figure 1 and 2)** was pressed into cylindrical pellets (1–2 mm thick, 13 mm diameter) by uniaxial pressing followed by isostatic pressing at 1000 kN. The green body pellets were covered in parent powder and sintered in alumina crucibles at 1070 °C for 10 h under $O_2$ atmosphere resulting in dense pellets of chemical composition c-$Li_{6.25}Al_{0.25}La_3Zr_2O_{12}$.

*$Li_4Ti_5O_{12}$ Electrode Slurry Preparation:* The electrode slurry was prepared by mixing carbon coated, nano-grained $Li_4Ti_5O_{12}$ (Life Power, Johnson Matthey), c-$Li_{6.25}Al_{0.25}La_3Zr_2O_{12}$ powder, conductive carbon (Super P, Li Timcal), and PVDF (Sigma-Aldrich) in the weight ratio 4:4:1:1 in an agate mortar. The powder mixture was dispersed in THF/toluene by ultrasonication.

In the following two sections, the processing of two different types of cells based on the above described c-$Li_{6.25}Al_{0.25}La_3Zr_2O_{12}$ pellets and $Li_4Ti_5O_{12}$ electrode slurry is described; the so-called *non-pressed cell* on the one hand and the *pressed cell* on the other:

*Preparation of non-pressed half battery cells $Li_4Ti_5O_{12}$ electrode/c-$Li_{6.25}Al_{0.25}La_3Zr_2O_{12}$ electrolyte:* For the non-pressed cells, dense c-$Li_{6.25}Al_{0.25}La_3Zr_2O_{12}$ pellets were polished down with P1200 sandpaper to a thickness of 360±20 µm and dried under vacuum before the $Li_4Ti_5O_{12}$ electrode slurry was cast onto the surface. After evaporation of the solvent for a few minutes, a weighting paper was put on top of the pellet and the electrode layer was consolidated by slightly pushing by hand. Subsequently the samples were dried completely under vacuum.

*Preparation of pressed half battery cells $Li_4Ti_5O_{12}$ electrode/c-$Li_{6.25}Al_{0.25}La_3Zr_2O_{12}$ electrolyte:* For the pressed cells, dense c-$Li_{6.25}Al_{0.25}La_3Zr_2O_{12}$ pellets were polished down and dried under vacuum. The electrode slurry was applied in the same way as for reference samples. Instead of applying slight pressure by hand, the samples were dried directly under vacuum before being folded into a single layer of aluminum foil. This is done to eliminate the possibility of electrode material sticking to the polymer wrapper during isostatic pressing. The samples were than pressed in isostatic mode at 1000 kN for 4 min. The aluminum foil was carefully removed afterwards.

*Assembly of All-Solid-State Battery Cells based on $Li_4Ti_5O_{12}$ electrode/c-$Li_{6.25}Al_{0.25}La_3Zr_2O_{12}$ electrolyte for pressed and non-pressed arrangements:* All-solid-state batteries of non-pressed and pressed cells were assembled in standard Swagelok-type cells in an Ar-filled glovebox. Li-metal counter electrodes were prepared from 0.75 mm Li foil (Alfa Aesar), resulting in all-solid-state cells of configuration $Li_4Ti_5O_{12}$ electrode / c-$Li_{6.25}Al_{0.25}La_3Zr_2O_{12}$ / Li-metal for both pressed and non-pressed arrangements.

"The synthesis, calcination, and sintering of c-$Li_{6.25}Al_{0.25}Zr_2O_{12}$ powder and pellets", and "the assembly of all-solid-state batteries" are in accordance to our previous paper on interface-engineered all-solid-state Li-ion batteries based on Al-doped LLZO [32]. Please also refer to it for a more detailed description of the specific steps mentioned above.

*Chemical and Structural Characterization:* Powder X-ray diffraction patterns of sintered pellets were obtained by crushing a sintered pellet in an agate mortar followed by analysis of the powder in a STOE Stadi P diffractometer equipped with a germanium monochromator and $CuK_\alpha$ radiation operated at 35 mA and 35 kV. SEM images of cross-sections of sintered c-$Li_{6.25}Al_{0.25}La_3Zr_2O_{12}$ pellets with $Li_4Ti_5O_{12}$ electrode layers were recorded for reference and pressed samples with a Zeiss Gemini 1530 operated at 5 kV.

*Electrochemical Impedance and All-Solid-State Battery Performance Tests:* Electrochemical impedance spectra were recorded at 95 °C with a Gamry Reference 600 potentiostat/galvanostat/ZRA in the frequency range of 1 MHz to 0.1 Hz with an alternating voltage of 10 mV against their open circuit potential. Battery performance was assessed by discharging and charging of both battery arrangements, either based on the non-pressed or on the pressed battery cell arrangement, in galvanostatic mode between 2.5 to 1.0 V at current rates of 2 and 8 A/kg at 95 °C.

## 3. Results and Discussion

Electrolyte pellets of composition c-$Li_{6.25}Al_{0.25}La_3Zr_2O_{12}$ have been used for all the battery cell configurations tested in this work. For the synthesis of the sub-micron sized c-$Li_{6.25}Al_{0.25}La_3Zr_2O_{12}$ a modified sol-gel synthesis-combustion method was used that had been first reported for Ga-doped LLZO [40]. Electrolyte pellets pressed and sintered from this powder showed a relative density of 87 ± 3 % and ionic conductivity of 5 x $10^{-4}$ S/cm that can be considered as sufficiently good for their use as solid electrolyte for all-solid-state batteries. Further details on the synthesis, processing, and characterization of the electrolyte pellets are given in our earlier work [32] and in Supporting Information. The $Li_4Ti_5O_{12}$ electrodes were deposited on sintered pellets by drop casting of a composite electrode slurry for both types of battery cells being either in the *non-pressed or pressed battery cell arrangement*. After drying off the solvent, the next step differs for the two battery types processed in this work, see **Figure 1**: The *non-pressed battery cell* serves mainly as a reference and is processed without any isostatic pressing step or interface modification. In contrast, the *pressed battery cell* was pressed isostatically to compact the electrode powder layer to the underlying electrolyte pellet. In the next step, full battery cells were assembled using metallic lithium as counter electrode in the same way for both non-pressed and pressed cells.

We turn to SEM cross-sections of battery cells for both arrangements to analyze the interface of $Li_4Ti_5O_{12}$ electrode–LLZO electrolyte and their microstructures, see **Figure 2a, 2b**. The non-pressed cell (**Figure 2a**) shows the $Li_4Ti_5O_{12}$ electrode as a rather loose powder layer of ~15-20 µm thickness with a very poor contact and bonding to the LLZO electrolyte pellet underneath. The electrode layer features a quite rough surface as only slight pressure was applied to the electrode with a finger. Individual electrode components are clearly

distinguishable from each other in this loose electrode powder mixture. In contrast, the pressed cell (**Figure 2b**) features a dense and well-contacted electrode layer towards the LLZO electrolyte and within the electrode structure itself. Here, the electrode composite is clearly seen as a graded continuing structure of the whole cell and is well compacted into a dense layer featuring not only a much better contact between the different electrode constituents but also between the electrode layer and the electrolyte. Here, a much smoother electrode surface is observed as a direct consequence of the isostatic pressing performed.

The effect of the different processing of the two $Li_4Ti_5O_{12}$ / c-$Li_{6.25}Al_{0.25}La_3Zr_2O_{12}$ / Li cell assemblies on the cell impedance and battery performance is analyzed by electrochemical impedance measurements and galvanostatic cycling of both assemblies. For the galvanostatic charge/discharge tests, the cells were cycled between 2.5 V and 1.0 V at 95 $^{\circ}$C with current rates of 2 and 8 Ah/kg respectively, see **Figure 3a, 3b**. The *non-pressed battery cells* are electrochemically active, however, deliver only limited capacities of ~1-2 Ah/kg with apparent polarization even at a relatively slow rate of 2 A/kg, see **Figure 3a**. In the case of *non-pressed cells* the Li-diffusion is simply hampered at the electrode-electrolyte interface due to poor contact, whereas the *pressed battery cells* show remarkable discharge capacities in the range of 75 Ah/kg when operated within 2.5 to 1.0 V at a high rate of 8 A/kg, see **Figure 3b**. The reversible lithiation/delithiation of $Li_4Ti_5O_{12}$ can be clearly tracked with distinct charge/discharge plateaus manifesting themselves as oxidation and reduction peaks at the dQ/dV plots of pressed-cells. The oxidation and reduction peaks appear at ~1.6 V and ~1.5 V respectively, see **Figure 4a**, matching well to the comparable liquid and solid electrolyte batteries based on $Li_4Ti_5O_{12}$ [32, 41]. The cycling is also fairly stable for a such solid-state battery system with a discharge capacity loss of ~1.4 % per cycle within the first 15 cycles, see **Figure 4b**. Though the coulombic efficiency is rather low at the 1st cycle with ~ 64 %, it recovers to ~ 74 % after 15 cycles, see **Supplementary Figure 3**. It should be noted that the achieved capacities here for the pressed-cells are highest among the

investigations applying direct casting methods on LLZO pellets [22, 32, 36, 37] and thereby emphasize once again the importance of reducing cell-impedances by the intimate embedding of the electrode particles into the solid electrolyte. In addition, specifically for $Li_4Ti_5O_{12}$ electrodes in full-ceramic LLZO batteries, the highest reported capacity of ~ 15 Ah/kg [32] has been increased here to ~75 Ah/kg for the discharge capacity of the 1$^{st}$ cycle. The post-mortem analysis of cycled cells with the same composition used in an earlier study revealed no new phases containing titanium at the electrolyte-electrode interface [32]. The stable cycling presented here with a relatively low discharge capacity loss also corroborates these results.

The analysis of the AC impedance spectra further confirms the improved contacting and reduced resistances for the pressed battery cell arrangement. Nyquist plots for the pressed and non-pressed cells are illustrated in **Figure 5**. The observed impedance semi-circles can be fitted with an equivalent circuit of a resistor and a constant phase element in parallel, and the outer intersection of the semi-circle with the real axis has been estimated as the total resistance of cells. It can be observed that the resistance values for the pressed cells are reduced by one order of magnitude when compared to the non-pressed battery cells; and even lower than the values where an additional interface modification but no isostatic pressing had been applied to the all-solid-state cells [32]. As here the sole difference between samples is the isostatic pressing of cells, the decrease in the overall resistance values can be directly attributed to the effect of pressing; consequently, resulting in an intimate embedding of the grains at the electrode-electrolyte interface and a better contacting. The pressed cells have a dense and well-integrated connection of the electrode into the solid-electrolyte; thereby reducing main impedances caused by the electrode – electrolyte interface and enabling the charge transfer.

From a ceramic processing perspective, this finding is a step forward in the field, as we report that half of the theoretical capacity for an electrode material can be achieved for an all-solid-state battery based on a Li-garnet electrolyte such as c-$Li_{6.25}Al_{0.25}La_3Zr_2O_{12}$. Compared to the previous investigations, the enhanced electrochemical properties reported here demonstrate the clear need to better ceramic bonding at the interface, which is achieved here by isostatic pressing of the cells. We suggest that a combination of interface modifications and pressing of cells could further boost the electrochemical performances of Li-garnet based all-solid batteries close to the theoretical capacities for various electrode materials at higher rates and lower operation temperatures. In addition, varying the thickness and morphology of applied electrode materials and finding an optimum processing ratio between the electrode and the solid electrolyte materials in the electrode mixture can be outlined as important focus points to further improve such all-solid-state Li-ion batteries in the future.

## 4. Conclusion

All-solid-state Li-ion batteries based on the garnet-type solid electrolyte c-$Li_{6.25}Al_{0.25}La_3Zr_2O_{12}$ (LZZO) were successfully fabricated and cycled with the anode material $Li_4Ti_5O_{12}$ for battery arrangements of $Li_4Ti_5O_{12}$-LLZO-Li. We report, for a *pressed battery processing arrangement*, high discharge capacities in the range of 75 Ah/kg for cycling within 2.5-1.0 V at 95 °C with a relatively high current rate of 8 A/kg. Notably, *i.* the performance of the cell is at half of the theoretical capacity for a full ceramic battery cell arrangement and *ii.* to the best of our knowledge, the battery capacity is the highest reported so far applying cheap direct casting methods for electrode fabrication on sintered LLZO pellets. We conclude that the choice of ceramic processing largely defines the impedances at the electrolyte-electrode interface in solid state, the grain embedment, and finally the performance of Li-transfer at the interface. The effect of isostatic pressing vs. direct application of the electrode slurry on the electrochemical impedance of the battery cell, their cell potentials, dQ/dV, and capacities are presented. By applying a relatively simple isostatic pressing of the solid electrolyte and the electrode, half of the theoretical capacity of an electrode material can be reached for all-solid-state Li-ion batteries with garnet-type solid electrolyte for the first time in large scale. Therefore, this investigation shows the importance of the electrode–solid electrolyte interface for all-solid-state batteries and is an important step towards the goal of reaching the maximum capacity of all-solid-state batteries based on garnet-type electrolytes with casted electrodes in the future.

**Acknowledgement**

The authors thank Competence Center Energy and Mobility (CCEM) and Alstom for funding of the projects: Proposal 911 “All Solid State Li-Ion Batteries based on New Ceramic Li-Ion Electrolytes” and SP-ESC-A 03-14, ETH Zürich Foundation “All Solid State Li+ Batteries with high Thermal Operation Window”, respectively.

**Figures**

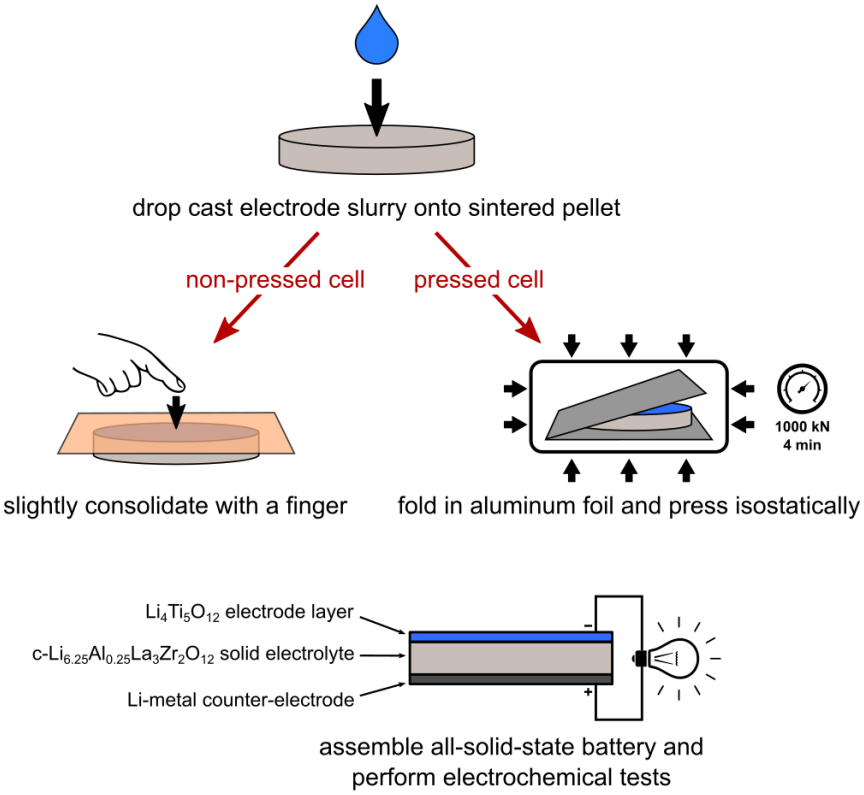


**Figure 1.** Schematic drawing of the electrode deposition via drop casting of an electrode composite slurry and the different processing of non-pressed and pressed cell types. Also shown is the final assembly of an all-solid-state batteries used for electrochemical characterization.

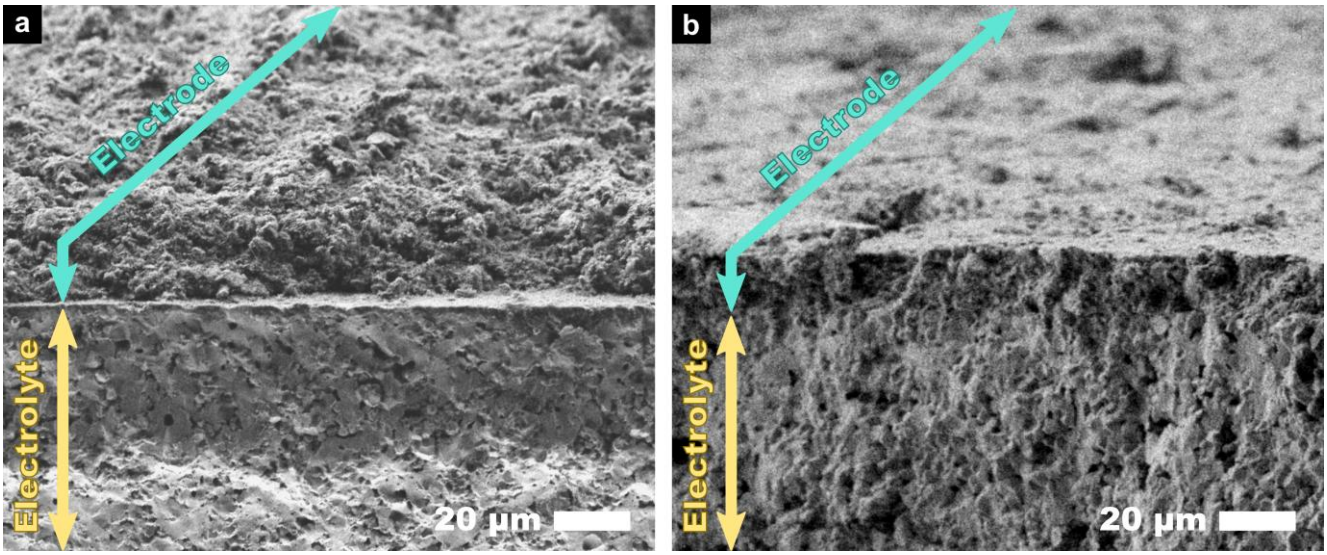


**Figure 2.** Scanning electron microscopy (SEM) images of as-assembled (a) *non-pressed* and (b) *pressed cell* cross-sections showing the c-$Li_{6.25}Al_{0.25}La_3Zr_2O_{12}$ electrolyte pellet with cast $Li_4Ti_5O_{12}$ electrode composite layer.

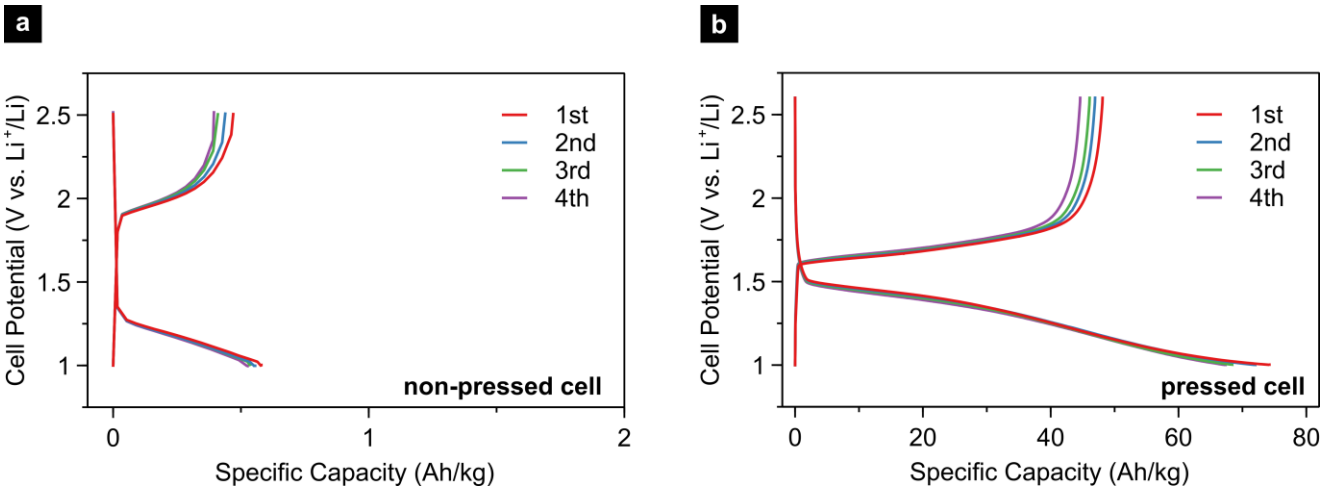


**Figure 3** (a) Galvanostatic charge/discharge curves for *non-pressed cells* at a current rate of 2 A/kg, (b) Galvanostatic charge/discharge curves for *pressed cells* at a current rate of 8 A/kg.

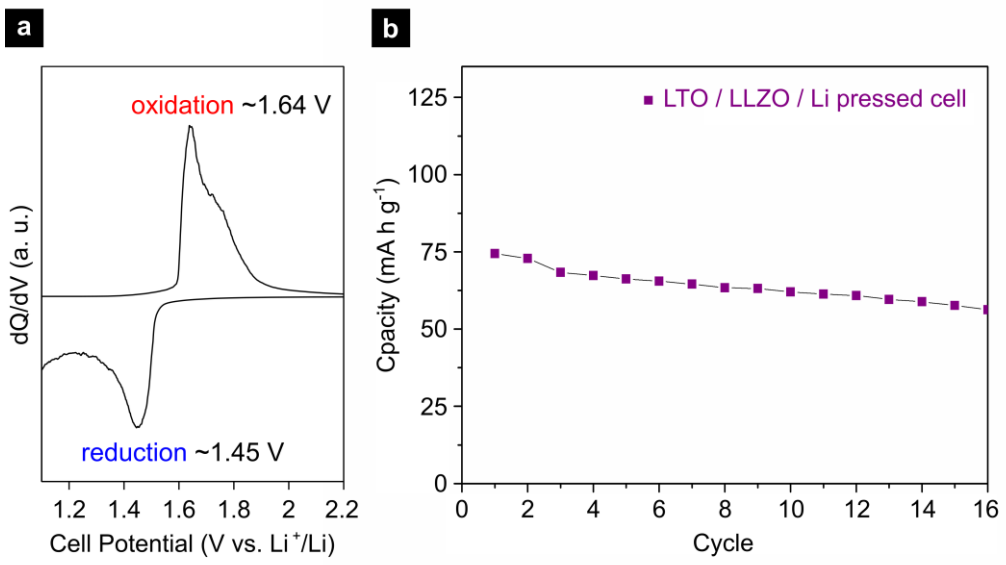


**Figure 4** (a) dQ/dV plot of a pressed cell showing clearly defined oxidation and reduction peaks, (b) Discharge capacity vs. cycle number for the $Li_4Ti_5O_{12}$ / c-$Li_{6.25}Al_{0.25}La_3Zr_2O_{12}$ / Li all-solid-state pressed cell at a rate of 8 A/kg within 2.5–1.0 V.

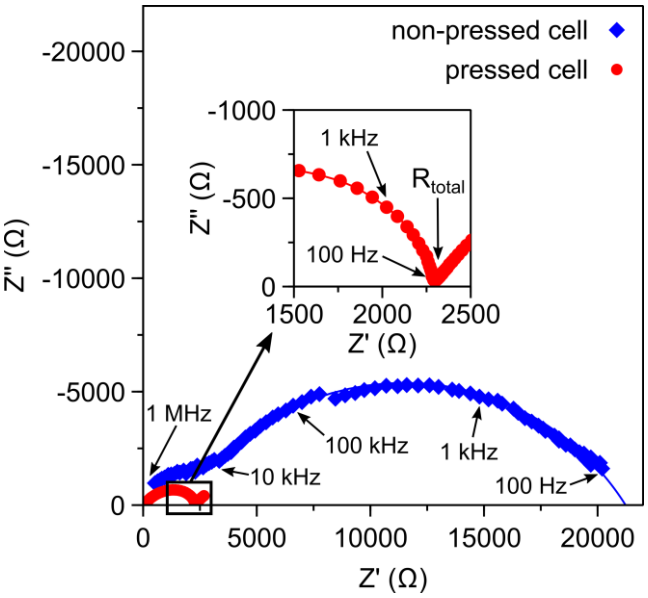


**Figure 5** Nyquist plots of *non-pressed* (blue) and *pressed* (red) cells of c-$Li_{6.25}Al_{0.25}La_3Zr_2O_{12}$ with nano-grained $Li_4Ti_5O_{12}$ and Li-metal electrodes measured at 95 °C

## References


1. Tarascon, J.M., M. Armand, Nature **414**, 359-67 (2001)
2. Bruce, P.G., S.A. Freunberger, L.J. Hardwick, J.M. Tarascon, Nat. Mater. **11**, 19-29 (2011)
3. Hayner, C.M., X. Zhao, H.H. Kung, Annu. Rev. Chem. Biomol. Eng. **3**, 445-71 (2012)
4. Ji, X., K.T. Lee, L.F. Nazar, Nat. Mater. **8**, 500-6 (2009)
5. Afyon, S., D. Kundu, A.J. Darbandi, H. Hahn, F. Krumeich, R. Nesper, J. Mater. Chem. A **2**, 18946-18951 (2014)
6. Afyon, S., M. Worle, R. Nesper, Angew. Chem., Int. Ed. Engl. **52**, 12541-4 (2013)
7. Perea, A., K. Zaghib, D. Bélanger, J. Mater. Chem. A **3**, 2776-2783 (2015)
8. Afyon, S., F. Krumeich, C. Mensing, A. Borgschulte, R. Nesper, Sci. Rep. **4**, 7113 (2014)
9. Moss, P.L., R. Fu, G. Au, E.J. Plichta, Y. Xin, J.P. Zheng, J. Power Sources **124**, 261-265 (2003)
10. Larcher, D., J.M. Tarascon, Nat. Chem. **7**, 19-29 (2015)
11. Wang, Y., W.-H. Zhong, ChemElectroChem **2**, 22-36 (2015)
12. Wang, Y., B. Liu, Q. Li, S. Cartmell, S. Ferrara, Z.D. Deng, J. Xiao, J. Power Sources **286**, 330-345 (2015)
13. Oudenhoven, J.F.M., L. Baggetto, P.H.L. Notten, Adv. Energy Mater. **1**, 10-33 (2011)
14. Kubicek, M., R. Schmitt, F. Messerschmitt, J.L.M. Rupp, ACS Nano **9**, 10737-10748 (2015)
15. Messerschmitt, F., M. Kubicek, S. Schweiger, J.L.M. Rupp, Advanced Functional Materials **24**, 7448-7460 (2014)
16. Cao, C., Z.-B. Li, X.-L. Wang, X.-B. Zhao, W.-Q. Han, Front. Energy Res. **2**, (2014)
17. Knauth, P., Solid State Ionics **180**, 911-916 (2009)
18. Janek, J., W.G. Zeier, Nat. Energy **1**, 16141 (2016)
19. Murugan, R., V. Thangadurai, W. Weppner, Angew. Chem., Int. Ed. Engl. **46**, 7778-81 (2007)
20. Thangadurai, V., S. Narayanan, D. Pinzaru, Chem. Soc. Rev. **43**, 4714-27 (2014)
21. Kotobuki, M., K. Kanamura, Y. Sato, T. Yoshida, J. Power Sources **196**, 7750-7754 (2011)
22. Kotobuki, M., H. Munakata, K. Kanamura, Y. Sato, T. Yoshida, J. Electrochem. Soc. **157**, A1076 (2010)
23. Geiger, C.A., E. Alekseev, B. Lazic, M. Fisch, T. Armbruster, R. Langner, M. Fechtelkord, N. Kim, T. Pettke, W. Weppner, Inorg. Chem. **50**, 1089-97 (2011)
24. Rangasamy, E., J. Wolfenstine, J. Sakamoto, Solid State Ionics **206**, 28-32 (2012)
25. Jin, Y., P.J. McGinn, J. Power Sources **196**, 8683-8687 (2011)
26. Zeier, W.G., Dalton Trans. **43**, 16133-8 (2014)
27. Hitz, G.T., E.D. Wachsman, V. Thangadurai, J. Electrochem. Soc. **160**, A1248-A1255 (2013)
28. Bernuy-Lopez, C., W. Manalastas, J.M. Lopez del Amo, A. Aguadero, F. Aguesse, J.A. Kilner, Chem. Mater. **26**, 3610-3617 (2014)
29. Jalem, R., Y. Yamamoto, H. Shiiba, M. Nakayama, H. Munakata, T. Kasuga, K. Kanamura, Chem. Mater. **25**, 425-430 (2013)
30. Rettenwander, D., P. Blaha, R. Laskowski, K. Schwarz, P. Bottke, M. Wilkening, C.A. Geiger, G. Amthauer, Chem. Mater. **26**, 2617-2623 (2014)
31. Buschmann, H., J. Dolle, S. Berendts, A. Kuhn, P. Bottke, M. Wilkening, P. Heitjans, A. Senyshyn, H. Ehrenberg, A. Lotnyk, V. Duppel, L. Kienle, J. Janek, Phys. Chem. Chem. Phys. **13**, 19378-92 (2011)
32. van den Broek, J., S. Afyon, J.L.M. Rupp, Adv. Energy Mater. **6**, 1600736 (2016)
33. Rawlence, M., I. Garbayo, S. Buecheler, J.L. Rupp, Nanoscale **8**, 14746-53 (2016)
34. Ohta, S., T. Kobayashi, J. Seki, T. Asaoka, J. Power Sources **202**, 332-335 (2012)
35. Ohta, S., T. Kobayashi, T. Asaoka, J. Power Sources **196**, 3342-3345 (2011)
36. Ohta, S., S. Komagata, J. Seki, T. Saeki, S. Morishita, T. Asaoka, J. Power Sources **238**, 53-56 (2013)
37. Ohta, S., J. Seki, Y. Yagi, Y. Kihira, T. Tani, T. Asaoka, J. Power Sources **265**, 40-44 (2014)

38. Kato, T., T. Hamanaka, K. Yamamoto, T. Hirayama, F. Sagane, M. Motoyama, Y. Iriyama, J. Power Sources **260**, 292-298 (2014)
39. Hansel, C., S. Afyon, J.L. Rupp, Nanoscale **8**, 18412-18420 (2016)
40. Afyon, S., F. Krumeich, J.L.M. Rupp, J. Mater. Chem. A **3**, 18636-18648 (2015)
41. Nowack, L.V., O. Waser, O. Yarema, V. Wood, RSC Adv. **3**, 15618 (2013)

## Supporting Information

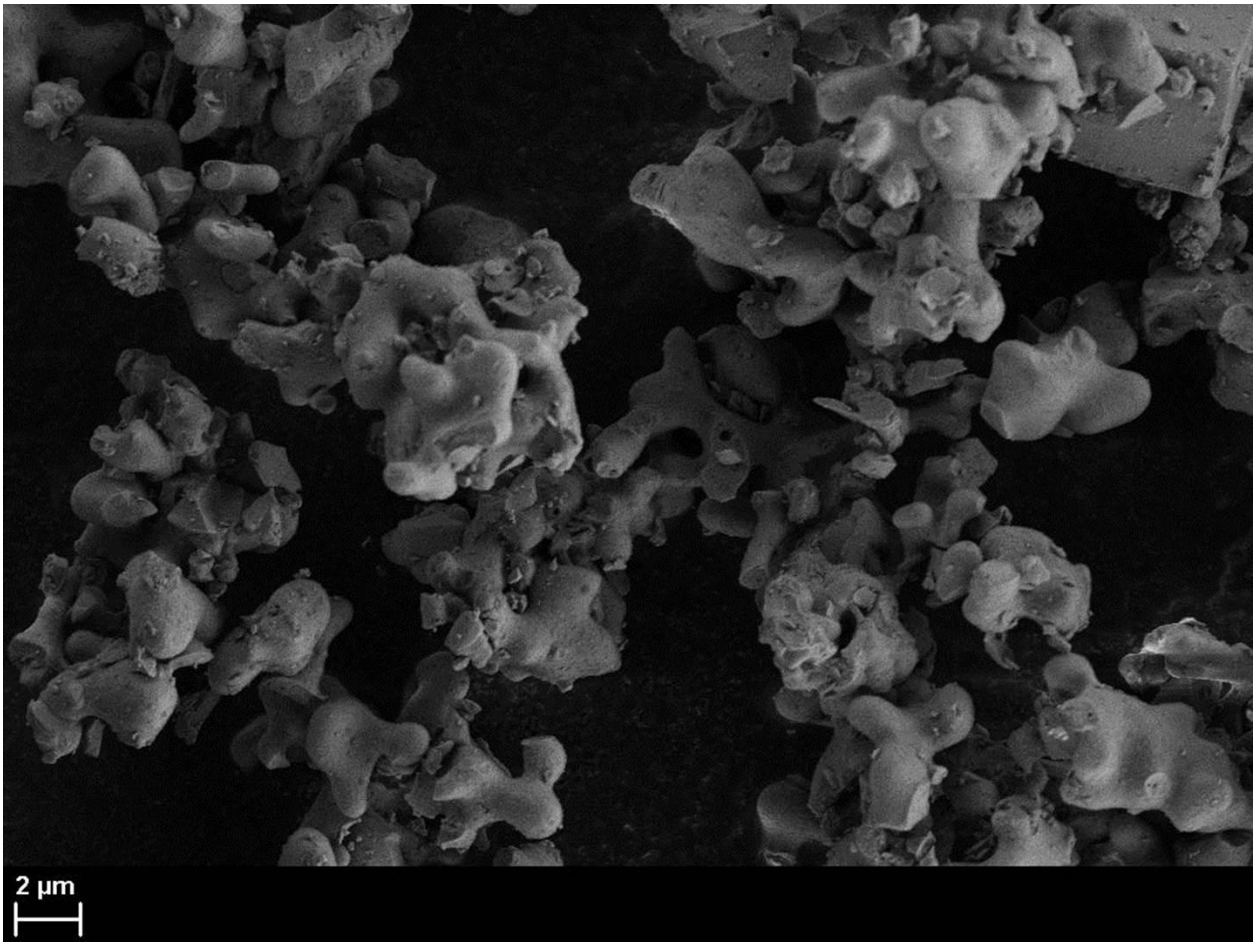


***Supplementary Figure 1:*** *Scanning electron microscopy (SEM) image of c-$Li_{6.25}Al_{0.25}La_3Zr_2O_{12}$, obtained after calcination of powder-gel at 650 °C.*

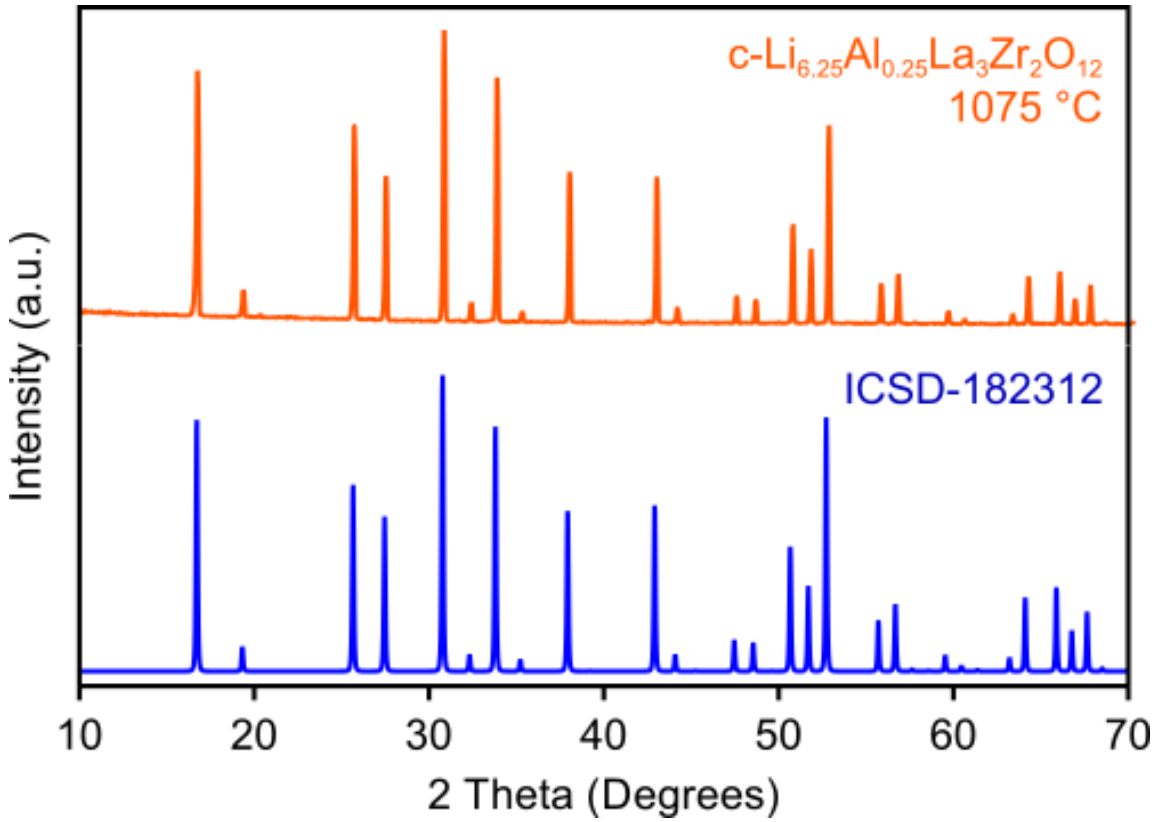


**Supplementary Figure 2:** XRD powder patterns of calculated c-$Li_7La_3Zr_2O_{12}$ (blue) and c-$Li_{6.25}Al_{0.25}La_3Zr_2O_{12}$ pellet after sintering (orange) respectively.

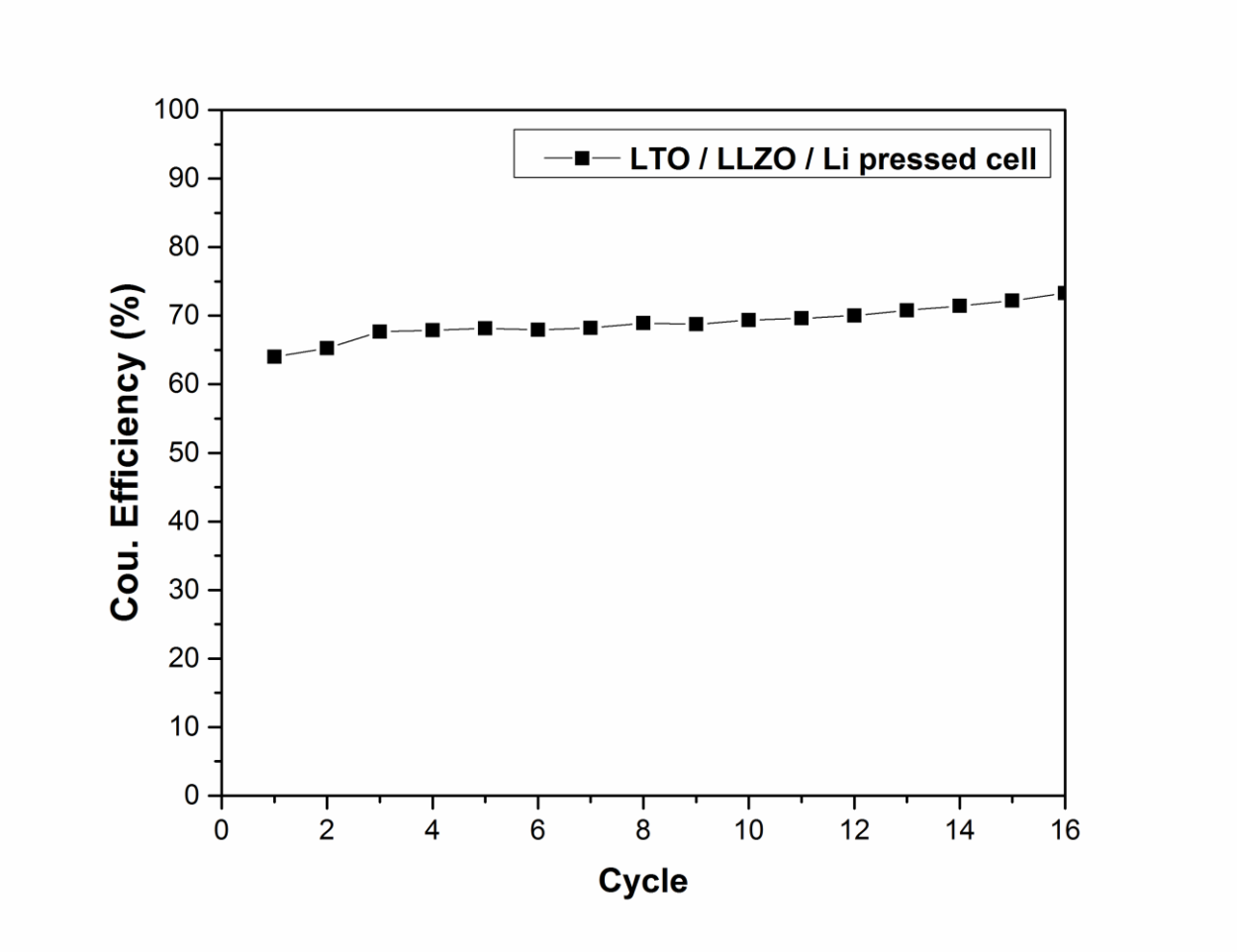


**Supplementary Figure 3:** Coulombic efficiency vs. cycle for the $Li_4Ti_5O_{12}$ / c-$Li_{6.25}Al_{0.25}La_3Zr_2O_{12}$ / Li all-solid-state pressed cell (shown in Figure 3 and 4) at a rate of 8 A/kg within 2.5–1.0 V.